ADVANCED MATERIALS
www.advmat.de

Stepwise On-Surface Synthesis and Transformations of Two-Dimensional Covalent Organic Frameworks by Controlled Thermal Stimuli

Ana Barragán, Elena Pérez-Elvira, Diego J. Vicent, Marco Lozano, Diego Soler-Polo, Koen Lauwaet, José M. Gallego, Rodolfo Miranda, José I. Urgel, Pavel Jelínek,* Nazario Martín,* and David Écija**

The development of covalent organic frameworks (COFs) is currently a primary objective in materials science, taking into account the envisioned applications in a variety of fields, including gas and energy storage, sensing, catalysis, and optoelectronics. Recently, the advent of on-surface covalent synthesis has allowed the design of one-atom-thick COFs, although the in situ transformations of such materials at interfaces have remained elusive. In this work, advantage is taken of an ex-professo synthesized molecular precursor endowed with gem-dibromide functional groups and a phenanthroline moiety to exploit steric hindrance as a synthetic controlling concept and, by subsequent chemical coupling reactions through thermal activation, afford COF transformations at interfaces in a controlled stepwise manner. In a first step, 1D covalent molecular chains are formed and self-assembled in a 2D supramolecular network, which, upon annealing, gives rise to a 2D porous organo-metallic network. Further annealing at higher temperatures affords the formation of a 2D-COF comprising linear chains based on ethynylene bridges at the cores of the monomers and carbon-carbon couplings at their peripheries. Such ethynylene linkages are transformed into antiaromatic pentalene moieties upon subsequent annealing, thus exemplifying the conversion of 2D-COFs at interfaces. These results provide new avenues toward the engineering and in situ chemical transformations of 2D-COFs in a stepwise manner, anticipating the tailoring of the structure and electronic properties of monolayer 2D-COFs by thermal stimuli.

1. Introduction

Covalent organic frameworks (COFs) are a class of highly ordered crystalline materials formed from molecular organic building units linked by covalent bonds. Their unique combination of properties, including high surface area, tunable pore, and remarkable chemical stability, have drawn enormous scientific and industrial attention in areas like gas storage, sensing, catalysis, drug delivery, and energy storage.[1–3]

Among the various types of COFs, 2D covalent organic frameworks (2D-COFs) have garnered significant attention for their unique layered and sheet-like structure. Herein, π–π interactions between stacked layers promote the mobility of electrons, making 2D-COFs excellent candidates for applications in electronics and optoelectronics, including sensors, supercapacitors, and solar cells.[4,5]

Despite the rapid advances in 2D-COF synthesis, several critical challenges remain unresolved. A key issue is the dynamic reversibility of the covalent bonds, which is essential for error correction during

A. Barragán, E. Pérez-Elvira, K. Lauwaet, R. Miranda, J. I. Urgel, N. Martín, D. Écija
Instituto Madrileño de Estudios Avanzados en Nanociencia (IMDEA Nanoscience)
Campus de Cantoblanco
C/ Faraday 9, Madrid 28049, Spain
E-mail: ana.barragan@imdea.org; nazmar@ucm.es; david.ecija@imdea.org

The ORCID identification number(s) for the author(s) of this article can be found under https://doi.org/10.1002/adma.202506942

DOI: 10.1002/adma.202506942

J. M. Gallego, J. I. Urgel, D. Écija
Unidad de Nanomateriales Avanzados
IMDEA Nanociencia
Unidad Asociada al CSIC por el ICMM
Campus de Cantoblanco
C/ Faraday 9, Madrid 28049, Spain

D. J. Vicent, N. Martín
Departamento de Química Orgánica
Facultad de Ciencias Químicas
Universidad Complutense de Madrid
Madrid 28040, Spain

M. Lozano, D. Soler-Polo, P. Jelínek
Institute of Physics of the Czech Academy of Science
Praha CZ-16253, Czech Republic
E-mail: jelinekp@fzu.cz

assembly yet difficult to control precisely without compromising structural stability. In parallel, achieving spatial control over the covalent linkages at the molecular level is an ongoing challenge; the lack of such control can lead to inhomogeneous pore distribution and suboptimal electronic properties. These limitations hamper the design of 2D-COFs with fully tailored functionalities and represent major obstacles in the field.[4]

Within the field of 2D-COFs, an enormous effort is set on reducing the thickness, thus affording 2D-COF nanosheets ranging from few- to single-layer materials.[6] The latter is particularly relevant for sensing and catalysis, considering that the entire materials would then be exposed to the environment, meaning all the surface is available for interaction with gases, liquids, or other substances. Additionally, electrons would be restricted to move within a 2D plane, which can enhance charge mobility and transport efficiency.[7] However, overcoming the challenges of dynamic bond reversibility and achieving precise spatial control remain pivotal for achieving these advantages.

The methods to produce 2D-COF nanosheets can be categorized as top-down or bottom-up. On one hand, the top-down strategy takes advantage of the exfoliation of the COF bulk, either by mechanical or liquid exfoliation. On the other hand, the bottom-up paradigm exploits the synthesis on a surface, including distinct environments such as ultra-high vacuum (UHV), vapor-assisted synthesis, and solid-liquid interface synthesis, or, alternatively, interfacial synthesis, either air/water or liquid/liquid interfaces.[6,7] In particular, on-surface synthesis under UHV conditions offers the design of monolayer 2D-COFs,[8–16] and the capability of characterizing the chemical structure of the material and its inherent electronic properties at the atomic scale thanks to the use of surface science techniques.[17,18]

A key aspect of the field is understanding how external stimuli can transform a pristine COF into a new COF with unique structural and electronic properties. Seminal examples have illustrated such challenges in bulk COFs.[19–23] However, to the best of our knowledge, the transformation of a monolayer 2D-COF at interfaces, where dynamic bond reversibility and spatial control are even more challenging, has remained elusive.

Here, we report a comprehensive scanning probe microscopy study, complemented by theoretical DFT simulations, about the synthesis and transformation of an unprecedented monolayer 2D-COF into another one on an Au(111) surface, going from ethynylene to pentalene bridges and peripheral carbon-carbon (C-C) coupling upon applying a thermal stimulus. To this aim, an ex-professo synthesized precursor equipped with gem-dibromide functional groups and a phenanthroline moiety is deposited on Au(111) and annealed to 150 °C, affording the formation of 1D ethynylene-based chains parallelly aligned through interstitial bromine atoms. A second annealing step promotes the Au-catalyzed C-H activation of specific hydrogens of the phenanthroline moiety and incorporates gold adatoms between the molecular wires, giving rise to a 2D organometallic network. Further annealing results in the C-C coupling among chains, affording a 2D-COF (**SURFCOF-IMDEA1**) with an electronic bandgap of 1.35 V. Finally, the last annealing step gives rise to ladderization of the molecular wires, allowing the formation of pentalene linkages, and also promoting further C-C coupling in between chains, altogether resulting in a distinct 2D-COF (**SURFCOF-IMDEA2**), with a reduced electronic bandgap of 0.90 V. Thus, this stepwise strategy not only addresses the inherent challenges of dynamic bond reversibility and spatial control over covalent linkages but also enables the tuning of the electronic band gap by 0.45 eV. These bandgap values position the reported materials within the moderate semiconductor range, a relatively rare and highly promising characteristic in the field of 2D-COFs. This range is ideal for achieving efficient charge carrier generation and controlled transport, effectively bridging the gap between materials with very wide bandgaps and those that are gapless. Moreover, the one-atom thickness of the COFs introduces pronounced quantum confinement effects, which may enhance their electronic and optical properties. The potential for even lower effective bandgaps underscores the tenability of these systems, which is critical for developing applications in nanoelectronics, optoelectronics, and energy conversion technologies.

Our results exemplify how to transform stepwise monolayer 2D-COFs at interfaces, overcoming key synthetic challenges and paving the way for future control of the structural and electronic properties of low-dimensional porous organic matter.

2. Synthesis of 2D Supramolecular Networks

Tetrabromo-*p*-quinodimethane precursor **1** (cf. **Scheme 1**) was synthesized following the procedure described in the Supporting Information (cf. Figures S1–S3, Supporting Information). The aim of this molecular design was to steer the polymerization through the activation of $=CBr_2$ moieties[24–26] and, simultaneously, exploiting the on-surface steric hindrance[27] and reactivity of the phenanthroline moieties, thus growing different 2D polymers in a thermally controlled sequential manner, as described below (cf. general Scheme 1).

The deposition of a submonolayer coverage of **1** on Au(111) held at room temperature (RT) under UHV conditions gives rise to patches of amorphous self-assembled pristine species (cf. Figure S4, Supporting Information). A first annealing step at 150 °C results in the formation of supramolecular nanoarchitectures based on 1D polymeric wires, as shown in the topographic scanning tunneling microscopy (STM) image shown in **Figure 1a**. A closer inspection reveals that the molecular precursors have lost their Br substituents, which are visualized as protrusions in the constant-current STM images,[24–26] and can be found either forming atomic chains over the surface or located in between the polymers (cf. Figure 1b), stabilizing a 2D supramolecular network, to be termed **phase *α***, with a projected average distance

J. M. Gallego
Instituto de Ciencia de Materiales de Madrid (ICMM)
CSIC
Cantoblanco
Madrid 28049, Spain
R. Miranda
Departamento de Física de la Materia Condensada
Universidad Autónoma de Madrid
Madrid 28049, Spain
P. Jelínek
Regional Centre of Advanced Technologies and Materials
Czech Advanced Technology and Research Institute (CATRIN)
Palacký University Olomouc
Olomouc 78371, Czech Republic

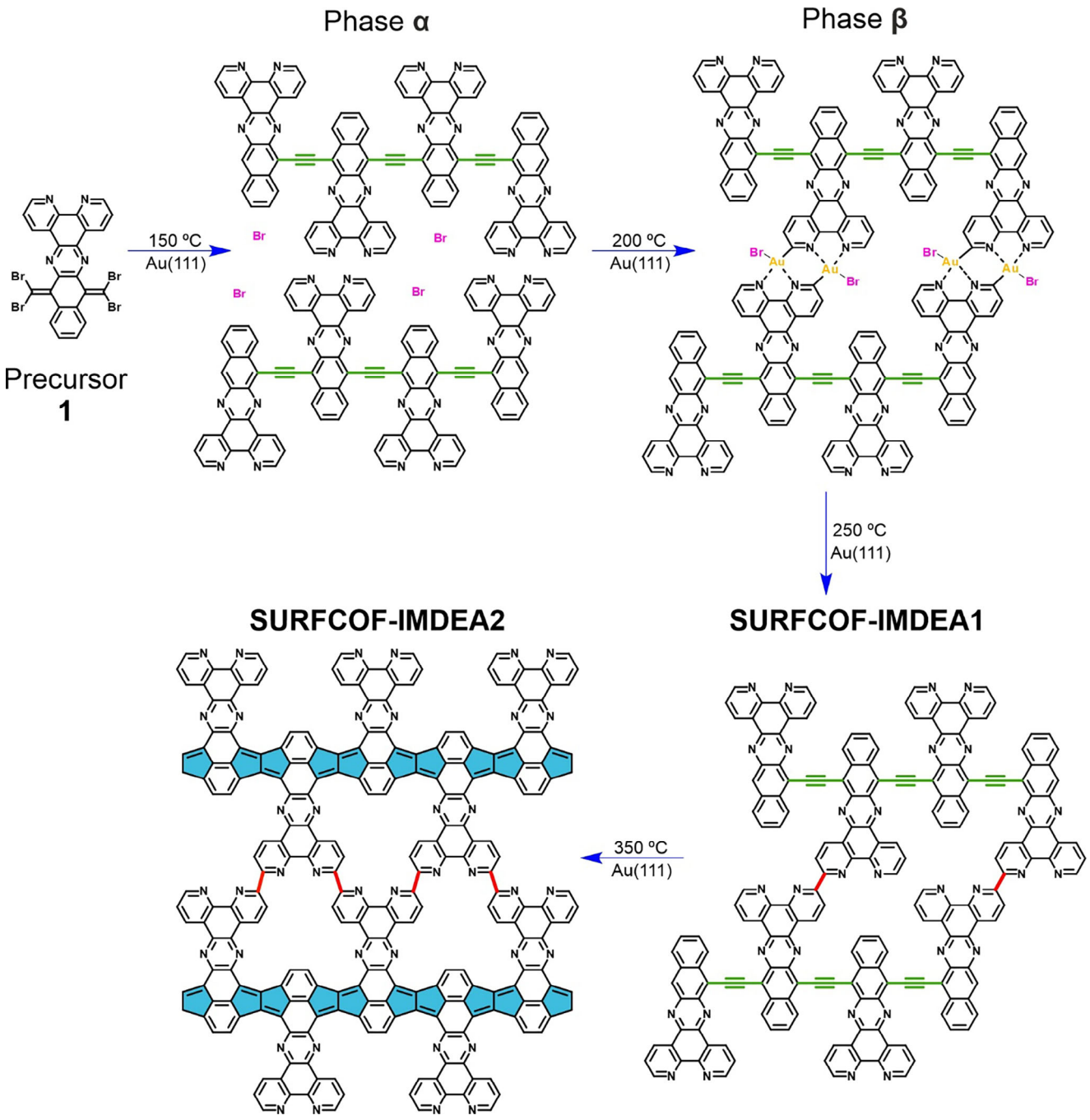

Scheme 1. Scheme of the chemical transformations of precursor **1** on Au(111) upon sequential steps of increasing thermal annealing, affording the formation of **SURFCOF-IMDEA1** and **SURFCOF-IMDEA2**, while illustrating the seminal 2D-COF to COF transformation on a metal surface. Ethynylene linkages are drawn in green, C-C couplings in red, and the formation of antiaromatic pentalene bridges is indicated in blue.

between parallel wires of ≈1.7 nm. High-resolution non-contact atomic force microscopy (nc-AFM) imaging acquired with a CO-tip allows us to discern the chemical structure of the monomers, which are linked to each other through ethynylene bridges, being the triple bond unambiguously distinguished as a bright protrusion for adequate tip-sample heights (cf. Figure 1c,d).[24,25] Monomers along the polymer alternate their orientation due to steric hindrance among adjacent species, although some defects can be observed (cf. Figure S5, Supporting Information). Importantly, most of the π-conjugated system of the monomer is adsorbed flat on the surface, whereas the peripheral rings of the phenanthroline units are visualized brighter and, thus, are slightly bent upward. At this stage, the molecular coverage is crucial since a large amount of Br intercalating in between the chains prevents the formation of defect-free **phase *α*** (cf. Figure S6, Supporting Information).

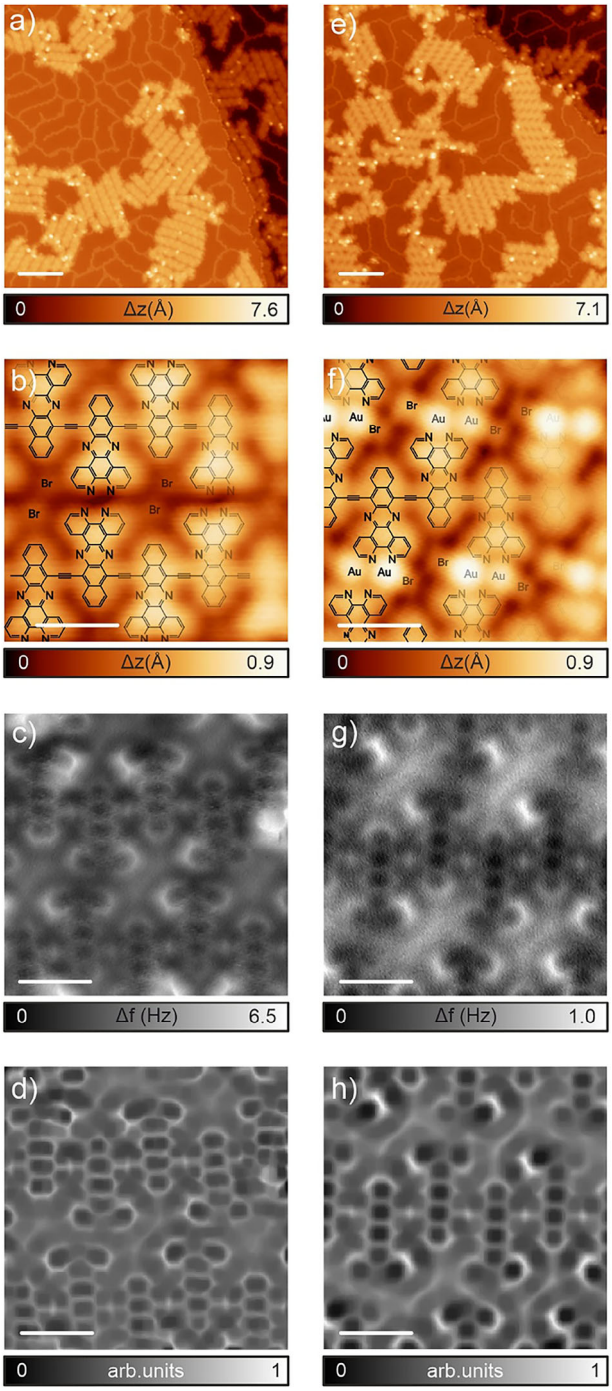

Figure 1. On-surface synthesis of supramolecular **phases** α and β on Au(111). a,e) Overview STM images after deposition of **1** on an Au(111) substrate and post-annealing at 150 and 200 °C, respectively. $V_b = -1.0$ V, $I_t = 80$ pA, scale bar: 10 nm, and $V_b = 0.5$ V, $I_t = 50$ pA, scale bar: 10 nm, respectively. b,f) Zoom-in constant-current STM images of **phases** α and β, respectively, with superimposed chemical structure sketches. $V_b = 0.05$ V, $I_t = 50$ pA, scale bar: 1 nm, and $V_b = -0.5$ V, $I_t = 50$ pA, scale bar: 1 nm, respectively. c,g) Constant-height frequency-shift nc-AFM images of **phases** α and β, respectively, acquired with a CO-functionalized tip. Z-offset: −80 and −60 pm, respectively, above STM set point (5 mV, 50 pA). d,h) Corresponding Laplace-filtered nc-AFM images.

A second annealing step at 200 °C preserves the 1D covalent nanoarchitecture, while Au adatoms promote the C—H activation of specific hydrogen atoms at the phenanthroline moieties, being incorporated into the pores of **phase** α (cf. Figure 1e,f), establishing organometallic complexes between the lone pairs of the two nitrogen atoms of the phenanthroline units in one wire and one carbon atom in the contiguous one, altogether resulting in a 2D porous organometallic network, to be termed **phase** β. It is worth mentioning that these organometallic complexes exhibit a Br atom attached to the Au adatom, and the whole Au-Br pair is visualized as two bright protrusions with STM (cf. Figure 1f). As a result of these organometallic linkages, the 1D covalent chains are slightly offset while facing adjacent pyridine peripheries, with an experimental distance between parallel chains of ≈1.9 nm, 0.2 nm larger than in **phase** α, due to the presence of gold adatoms. The high-resolution nc-AFM image shown in Figure 1g allows us to clearly resolve the ethynylene bridges, while the associated Laplace-filtered image in Figure 1h enables the detection of the bright protrusions assigned to the gold adatoms, corroborating the findings by STM. Complementary, nc-AFM images acquired at different tip-sample heights have also been included in Figure S7 (Supporting Information). Although many phenanthroline-based organometallic complexes have been synthesized using conventional wet chemistry methodologies[28] and their supramolecular complexation of metal adatoms on surfaces has been reported,[29] it is important to highlight that this is the first example of an on-surface synthesized 2D phenanthroline-containing organometallic network, which in this case is based on N2-Au-C bonds, i.e., an assembly stabilized by one metal-carbon bond and by two metal-nitrogen links from the phenanthroline functional group.

3. On-Surface Synthesis and Stepwise Transformations of 2D-COFs

The next annealing step at 250 °C results in the formation of single C—C bonds in between adjacent wires, which are now at a distance of ≈1.6 nm, in such a way that the C atom of the organometallic complex of each monomer establishes just one C-C linkage with the one in the antiparallel monomer, thus giving rise to a 2D-COF, to be termed **phase** γ in the text, and given the name of **SURFCOF-IMDEA1**. Large-scale STM images reveal the formation of small patches comprising **phase** γ, coexisting with defective organic material (less than 30%) and the desorption of Br atoms from the Au(111) surface (cf. **Figure 2a**). High-resolution STM images acquired at constant-current (cf. Figure 2b) and constant-height (cf. Figure 2c) display the formation of such C—C bond as a protrusion of similar contrast to the monomer backbone while preserving the integrity of the longitudinal covalent axis. Importantly, the Au adatoms are not detected, and the antiparallel monomers from adjacent wires are now displaced with respect to the axis of symmetry to establish the C—C bond. Nc-AFM images display that the periphery of the monomer not involved in the C-C linkage is non-planar and slightly out of the plane, being visualized as a bright line (cf. Figure 2d–f). In addition, the ethynylene bridge is still preserved. The match between experimental (cf. Figure 2d), Laplace-filtered

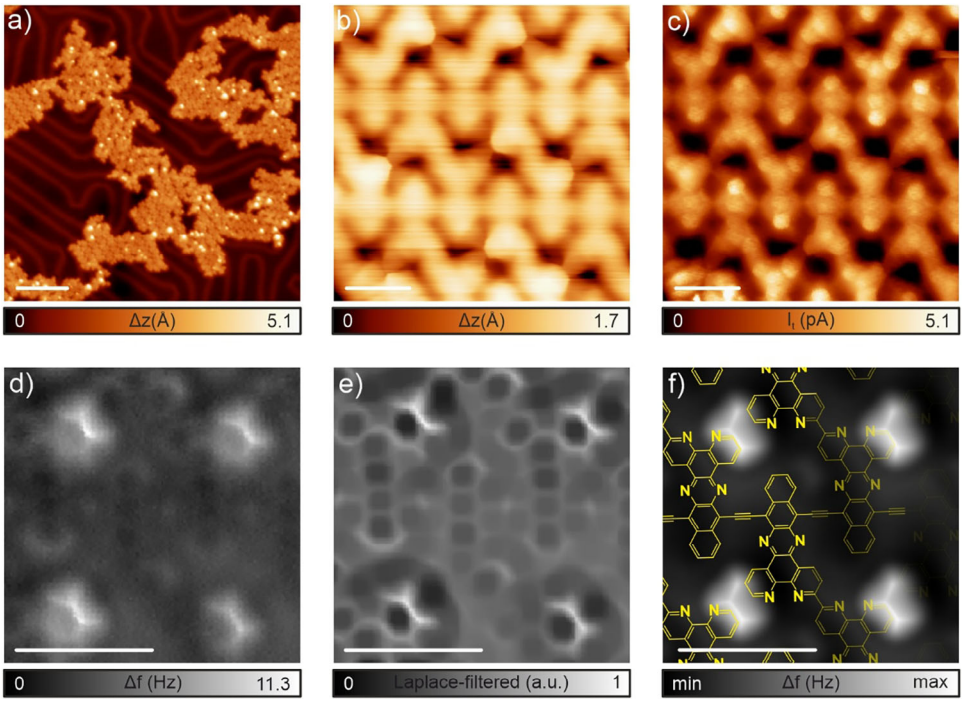

Figure 2. On-surface synthesis of 2D-COF **phase *γ*** on Au(111), named **SURFCOF-IMDEA1**, upon annealing **phase *β*** at 250 °C. a) Overview STM image. $V_b = 0.5$ V, $I_t = 50$ pA, scale bar: 10 nm b, c) Zoom-in constant-current and constant-height STM images, respectively. $V_b = 50$ mV, $I_t = 50$ pA, scale bar: 1 nm, and $V_b = 5$ mV, $I_t = 50$ pA, scale bar: 1 nm. d,e) Original and Laplace-filtered experimental nc-AFM images of a small patch, respectively. Z-offset: 60 pm above STM set point (5 mV, 50 pA), scale bar: 1 nm. f) Corresponding simulated nc-AFM image using PP-AFM code[30] with chemical structure superimposed.

(cf. Figure 2e), and calculated nc-AFM images (cf. Figure 2f) is excellent, ratifying our rationalization of the structure.

A final annealing step at 350 °C gives rise to the formation of **phase *δ***, which is also an unprecedented 2D porous COF (named **SURFCOF-IMDEA2**) and results from two concomitant reactions from **phase *γ***: i) the formation of an additional C-C coupling in between antiparallel adjacent monomers, and ii) the ladderization of the inner longitudinal covalent axis. The formation of small patches comprising **phase *γ*** is illustrated in **Figure 3a**, coexisting with defective material (less than 30%). High-resolution constant-current (cf. Figure 3b) and constant-height (cf. Figure 3c) STM images clearly display the ladderization of the longitudinal pathway, as previously illustrated from the annealing of cumulene-based bisanthene polymers.[26,31] In addition, the antiparallel monomers are now doubly connected by C—C bonds. Such assumptions are clearly confirmed by the acquired nc-AFM images where both the ladderization exemplified by a pentalene bridge, as well as the single C—C bonds seen as straight lines, are noticed. Notably, the ethynylene bridge has also been able to transform into antiaromatic pentalene bridges (cf. Figure S8, Supporting Information for experimental elucidation of the dominant resonant form), thus enhancing the portfolio to promote ladderization of organic polymers not only in one-, but in two-dimensions. Again, the agreement between experimental and calculated nc-AFM images is excellent (cf. Figure 3d–f), overall justifying the structure of **SURFCOF-IMDEA2**, which can be seen as a 2D porous COF, forming a triangular pore size of ≈0.55 nm^2, with potential relevance for hosting molecular adsorbates and, thus, to be used for organic templating and sensing.

The average morphology of phases **SURFCOF-IMDEA1** (**phase *γ***) and **SURFCOF-IMDEA2** (**phase *δ***) consisted of nanoislands with nearly rectangular shapes, typically measuring 10 nm by 20 nm. These nanoislands were almost defect-free at the interior, while their borders were decorated with amorphous matter. The yield of the nanomaterial was 75% and 78% for phases **SURFCOF-IMDEA1** and **SURFCOF-IMDEA2**, respectively (see Figure S9, Supporting Information and discussion about defects in Supporting Information). The average surface coverage of the phases was ≈0.3 ML, with higher coverages precluded due to coverage-dependent reactivity as discussed above (see Figures S6 and S9, Supporting Information).

Finally, we focus on the electronic properties of the two novel 2D-COFs to clarify how these properties are influenced by the reported chemical transformation. To this aim, we acquire scanning tunneling spectroscopy (STS) at selected locations within the 2D-COFs. According to our results (cf. **Figure 4a,b**), **SURFCOF-IMDEA1** displays four electronic resonances at −1.10, −0.65 V (onset of valence band), 0.70 V (onset of conduction band) and 1.30 V, being the resonance at around −0.30 V simply the displacement of the surface state of Au(111), which altogether would imply an electronic bandgap of ≈1.35 V (cf. Figure S10a, Supporting Information for dI/dV mapping of the onsets of the bands). Upon annealing such phase to give rise to **SURFCOF-IMDEA2** a clear transformation of the electronic structure is detected (cf. Figure 4c,d), being the onsets of the

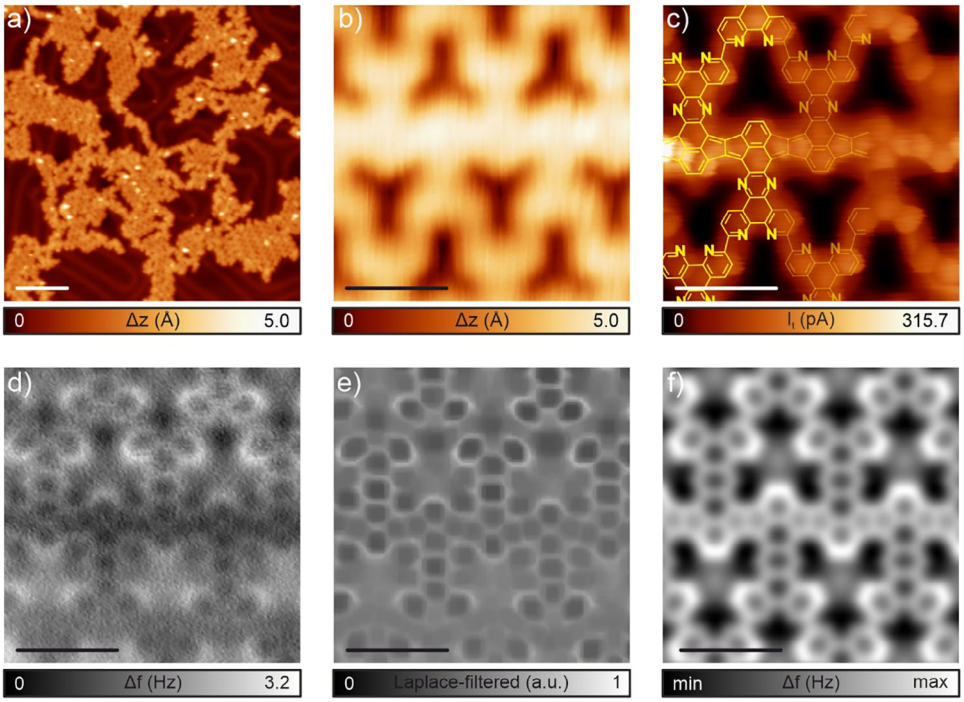

Figure 3. On-surface synthesis of **phase** δ on Au(111), named **SURFCOF-IMDEA2**, by annealing **phase** γ at 350 °C. a) Overview STM image. $V_b = 0.5$ V, $I_t = 50$ pA, scale bar: 10 nm. b,c) Zoom-in constant-current and constant-height STM images with the chemical structure superimposed, respectively. $V_b = 0.05$ V, $I_t = 50$ pA, scale bar: 1 nm, and $V_b = 5$ mV, $I_t = 50$ pA, scale bar: 1 nm. d,e) Original and Laplace-filtered experimental nc-AFM images of a small patch, respectively. Z-offset: 140 pm above STM set point (5 mV, 50 pA), scale bar: 1 nm. f) Corresponding simulated nc-AFM image using PP-AFM code.[30]

valence and conduction bands located at −0.60 and 0.30 V, respectively, thus reducing the electronic bandgap to 0.90 V (cf. Figure S10b, Supporting Information for dI/dV mapping of the onsets of the bands). This experimentally observed bandgap reduction could be accounted for by the experimental increase in planarity and π-conjugation as well as the presence of antiaromatic pentalene moieties (cf. Figure S10c,d, Supporting Information for further discussion therein about the electronic structure of both phases).

4. Conclusion

In summary, we report a comprehensive scanning probe microscopy study, complemented by theoretical calculations, on the synthesis of a 2D surface covalent organic network (**SURFCOF-IMDEA1**) and seminally exemplify its further controlled sequential transformation into a different 2D porous surface covalent network (**SURFCOF-IMDEA2**), by increasing the annealing temperature on the surface.

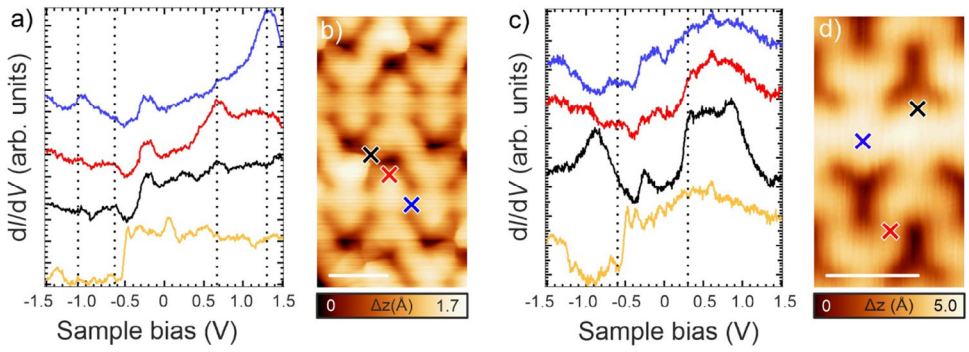

Figure 4. Electronic structure of **SURFCOF-IMDEA1** and **SURFCOF-IMDEA2**. a) dI/dV spectra of **SURFCOF-IMDEA1** acquired at the positions indicated by the blue, red, and black crosses in panel b, revealing an electronic bandgap of ≈1.35 V. b) **SURFCOF-IMDEA1** patch. $V_b = 0.05$ V, $I_t = 50$ pA, scale bar: 1 nm. c) dI/dV spectra of **SURFCOF-IMDEA1** acquired at the positions indicated in panel d, revealing a bandgap of 0.90 V. d) **SURFCOF-IMDEA2** patch. $V_b = 0.05$ V, $I_t = 50$ pA, scale bar: 1 nm. Reference spectrum (orange) was taken on the Au(111) surface for both phases. Open feedback parameters for dI/dV spectra: $V_b = 1.5$ V, $I_t = 300$ pA, $V_{rms} = 30$ mV.

To this aim, we have ex-professo synthesized precursor **1**, whose shape has been designed to tailor, using the steric hindrance concept and after a first annealing step at 150 °C, a former polymeric **phase *α*** based on 1D molecular wires featuring ethynylene bridges and comprising antiparallel monomers supramolecularly interacting through residual Br atoms. After a second annealing step at 200 °C, an unprecedented 2D organometallic network, **phase *β***, has been synthesized, in which Au adatoms come into play interacting with adjacent covalent molecular wires while preserving the ethynylene bridges, and aligning such wires into a parallel fashion through organometallic N_2-Au-C bonds. Next annealing to higher temperatures induces the first C-C linkage in between antiparallel monomers of adjacent molecular wires, resulting in the expression of **SURFCOF-IMDEA1** (**phase *γ***), which can be rationalized as a 2D-COF, featuring an electronic bandgap of 1.35 eV. A final annealing step at 350 °C results in a further ladderization of the longitudinal molecular wires through a transformation of the ethynylene bridge into antiaromatic pentalene linkages. Concomitantly, the peripheries of adjacent antiparallel monomers establish a second C—C bond, overall resulting in the 2D porous COF **SURFCOF-IMDEA2** (**phase *δ***), featuring an electronic bandgap of 0.90 eV.

As a result, simply by subsequent annealing steps, we illustrate the combined potential of supramolecular and on-surface covalent synthesis to trigger, in a controlled stepwise manner, the formation of surface-confined 2D supramolecular and covalent organic frameworks on a metal surface, and we seminally illustrate how to guide a 2D-COF to COF transformation on a surface, concomitantly changing not only the chemical structure but also the electronic properties.

Our findings pave new avenues for the controlled stepwise synthesis of 2D organic materials and illustrate a powerful strategy to covalently tailor such designs on surfaces, which we envision will have a potential impact in the fields of reticular chemistry, plastic electronics, and sensing.

Supporting Information

Supporting Information is available from the Wiley Online Library or from the author.

Acknowledgements

A.B., E.P.-E., and D.J.V. contributed equally to this work. This project had received funding from MCIN/AEI/10.13039/501100011033 through grants PID2019-108532GB-I00, PID2023-146373OB-I00 and PDC2023-145871-I00. The authors acknowledged the support from the "(MAD2D-CM)-IMDEA-Nanociencia" and "(MAD2D-CM)-UCM" projects funded by Comunidad de Madrid, by the Recovery, Transformation and Resilience Plan, and by NextGenerationEU from the European Union. The authors thanked Comunidad de Madrid through Programa de Actividades de I+D (TEC-2024/TEC-459, SYNMOLMAT-CM). D.J.V and N.M. also acknowledged financial support from the ERC (SyG TOMATTO) ERC-2020-951224). The authors appreciated funding from the CzechNanoLab Research Infrastructure supported by MEYS CR (LM2018110) and project GACR no. 23–05486S. J.I.U. acknowledged the funding from MCIU for the Ramón y Cajal (RYC2022-037352). A.B. acknowledged financial support from the Juan de la Cierva program (FJC2021-046524-I).

Conflict of Interest

The authors declare no conflict of interest.

Data Availability Statement

The data that support the findings of this study are available from the corresponding author upon reasonable request.

Keywords

covalent organic frameworks, on-surface synthesis, scanning probe microscopies

Received: April 11, 2025
Published online:

[1] A. P. Côté, A. I. Benin, N. W. Ockwig, M. O'Keeffe, A. J. Matzger, O. M. Yaghi, *Science* **2005**, *310*, 1166.
[2] J. Jiang, Y. Zhao, O. M. Yaghi, *J. Am. Chem. Soc.* **2016**, *138*, 3255.
[3] K. Geng, T. He, R. Liu, S. Dalapati, K. T. Tan, Z. Li, S. Tao, Y. Gong, Q. Jiang, D. Jiang, *Chem. Rev.* **2020**, *120*, 8814.
[4] R.-R. Liang, S.-Y. Jiang, R.-H. A., X. Zhao, *Chem. Soc. Rev.* **2020**, *49*, 3920.
[5] C. Wang, Z. Zhang, Y. Zhu, C. Yang, J. Wu, W. Hu, *Adv. Mater.* **2022**, *34*, 2102290.
[6] D. Rodríguez-San-Miguel, C. Montoro, F. Zamora, *Chem. Soc. Rev.* **2020**, *49*, 2291.
[7] J. Fan, Z. Wang, H. Cheng, D. Wang, A. T. Wee, *Electron. Mater.* **2023**, *4*, 49.
[8] N. A. A. Zwaneveld, R. Pawlak, M. Abel, D. Catalin, D. Gigmes, D. Bertin, L. Porte, *J. Am. Chem. Soc.* **2008**, *130*, 6678.
[9] L. Grill, M. Dyer, L. Lafferentz, M. Persson, M. V. Peters, S. Hecht, *Nat. Nanotechnol.* **2007**, *2*, 687.
[10] S. Clair, D. G. de Oteyza, *Chem. Rev.* **2019**, *119*, 4717.
[11] C. Moreno, M. Vilas-Varela, B. Kretz, A. Garcia-Lekue, M. V. Costache, M. Paradinas, M. Panighel, G. Ceballos, S. O. Valenzuela, D. Peña, A. Mugarza, *Science* **2018**, *360*, 199.
[12] Q. Fan, L. Yan, M. W. Tripp, O. Krejčí, S. Dimosthenous, S. R. Kachel, M. Chen, A. S. Foster, U. Koert, P. Liljeroth, J. M. Gottfried, *Science* **2021**, *372*, 852.
[13] G. Galeotti, F. De Marchi, E. Hamzehpoor, O. MacLean, M. R Rao, Y. Chen, L. V. Besteiro, D. Dettmann, L. Ferrari, F. Frezza, P. M. Sheverdyaeva, R. Liu, A. K. Kundu, P. Moras, M. Ebrahimi, M. C. Gallagher, F. Rosei, D. F. Perepichka, G. Contini, *Nat. Mater.* **2020**, *19*, 874.
[14] C. Chen, T. Joshi, H. Li, A. D. Chavez, Z. Pedramrazi, P.-N. Liu, H. Li, W. R. Dichtel, J.-L. Bredas, M. F. Crommie, *ACS Nano* **2018**, *12*, 385.
[15] D. Wang, Z. Wang, W. Liu, J. Z Arramel, Y. P. Feng, K. P. Loh, J. Wu, A. T. S. Wee, *ACS Nano* **2020**, *14*, 14008.
[16] C. Steiner, J. Gebhardt, M. Ammon, Z. Yang, A. Heidenreich, N. Hammer, A. Görling, M. Kivala, S. Maier, *Nat. Commun.* **2017**, *8*, 14765.
[17] C. Zhang, Z. Yi, W. Xu, *Mater. Futures* **2022**, *1*, 032301.
[18] N. Pavliček, L. Gross, *Nat. Rev. Chem.* **2017**, *1*, 0005.
[19] P. J. Waller, S. J. Lyle, T. M. Osborn Popp, C. S. Diercks, J. A. Reimer, O. M. Yaghi, *J. Am. Chem. Soc.* **2016**, *138*, 15519.
[20] H. Liu, J. Chu, Z. Yin, X. Cai, L. Zhuang, H. Deng, *Chem* **2018**, *4*, 1696.
[21] P. J. Waller, Y. S. AlFaraj, C. S. Diercks, N. N. Jarenwattananon, O. M. Yaghi, *J. Am. Chem. Soc.* **2018**, *140*, 9099.
[22] F. Haase, E. Troschke, G. Savasci, T. Banerjee, V. Duppel, S. Dörfler, M. M. J. Grundei, A. M. Burow, C. Ochsenfeld, S. Kaskel, B. V. Lotsch, *Nat. Commun.* **2018**, *9*, 2600.

[23] Z. Mu, Y. Zhu, Y. Zhang, A. Dong, C. Xing, Z. Niu, B. Wang, X. Feng, *Angew. Chem., Int. Ed.* **2023**, *62*, 202300373.
[24] A. Sánchez-Grande, B. de la Torre, J. Santos, B. Cirera, K. Lauwaet, T. Chutora, S. Edalatmanesh, P. Mutombo, J. Rosen, R. Zboril, R. Miranda, J. Björk, P. Jelínek, N. Martín, D. Ecija, *Angew. Chem., Int. Ed.* **2019**, *58*, 6559.
[25] B. Cirera, A. Sánchez-Grande, B. d. l. Torre, J. Santos, S. Edalatmanesh, E. Rodríguez-Sánchez, K. Lauwaet, B. Mallada, R. Zboril, R. Miranda, O. Gröning, P. Jelínek, N. Martín, D. Ecija, *Nat. Nanotechnol.* **2020**, *15*, 437.
[26] J. I. Urgel, A. Sánchez-Grande, D. J. Vicent, P. Jelínek, N. Martín, D. Écija, *Adv. Mater.* **2024**, *36*, 2402467.
[27] P. Ruffieux, S. Wang, B. Yang, C. Sánchez-Sánchez, J. Liu, T. Dienel, L. Talirz, P. Shinde, C. A. Pignedoli, D. Passerone, T. Dumslaff, X. Feng, K. Müllen, R. Fasel, *Nature* **2016**, *531*, 489.
[28] M. Shiotsuka, T. Asano, Y. Kurono, R. Ono, R. Kawabe, *J. Organomet. Chem.* **2017**, *851*, 1.
[29] H. Jiang, J. Lu, F. Zheng, Z. Zhu, Y. Yan, Q. Sun, *Chem. Commun.* **2023**, *59*, 8067.
[30] P. Hapala, G. Kichin, C. Wagner, F. S. Tautz, R. Temirov, P. Jelínek, *Phys. Rev. B* **2014**, *90*, 085421.
[31] B. de la Torre, A. Matěj, A. Sánchez-Grande, B. Cirera, B. Mallada, E. Rodríguez-Sánchez, J. Santos, J. I. Mendieta-Moreno, S. Edalatmanesh, K. Lauwaet, M. Otyepka, M. Medveď, Á. Buendía, R. Miranda, N. Martín, P. Jelínek, D. Écija, *Nat. Commun.* **2020**, *11*, 4567.